Biochimica et Biophysica Acta 1838 (2014) 56–68

Contents lists available at ScienceDirect

Biochimica et Biophysica Acta

journal homepage: www.elsevier.com/locate/bbamem

Review

Atomic force microscopy: A multifaceted tool to study membrane proteins and their interactions with ligands☆

Allison M. Whited, Paul S.-H. Park *

Department of Ophthalmology and Visual Sciences, Case Western Reserve University, Cleveland, OH 44106, USA

ARTICLE INFO

Article history:
Received 4 February 2013
Received in revised form 22 March 2013
Accepted 9 April 2013
Available online 16 April 2013

Keywords:
Imaging
Force spectroscopy
Molecular interaction
Energy landscape
Protein structure

ABSTRACT

Membrane proteins are embedded in lipid bilayers and facilitate the communication between the external environment and the interior of the cell. This communication is often mediated by the binding of ligands to the membrane protein. Understanding the nature of the interaction between a ligand and a membrane protein is required to both understand the mechanism of action of these proteins and for the development of novel pharmacological drugs. The highly hydrophobic nature of membrane proteins and the requirement of a lipid bilayer for native function have hampered the structural and molecular characterizations of these proteins under physiologically relevant conditions. Atomic force microscopy offers a solution to studying membrane proteins and their interactions with ligands under physiologically relevant conditions and can provide novel insights about the nature of these critical molecular interactions that facilitate cellular communication. In this review, we provide an overview of the atomic force microscopy technique and discuss its application in the study of a variety of questions related to the interaction between a membrane protein and a ligand. This article is part of a Special Issue entitled: Structural and biophysical characterization of membrane protein–ligand binding.

Contents

Abbreviations: AFM, atomic force microscopy; DFS, dynamic single-molecule force spectroscopy; F–D, force–distance; GPCR, G protein-coupled receptor; HOPG, highly ordered pyrolytic graphite; ICAM-1, intercellular adhesion molecule-1; LFA-1, leukocyte function-associated antigen-1; LHRH, luteinizing hormone-releasing hormone; PE40, *Pseudomonas aeruginosa* exotoxin 40; SMFS, single-molecule force spectroscopy; STM, scanning tunneling microscopy

☆ This article is part of a Special Issue entitled: Structural and biophysical characterization of membrane protein–ligand binding.

* Corresponding author. Tel.: +1 216 368 2533; fax: +1 216 368 3171.
E-mail address: paul.park@case.edu (P.S.-H. Park).

0005-2736/$ – see front matter © 2013 Elsevier B.V. All rights reserved.
http://dx.doi.org/10.1016/j.bbamem.2013.04.011

1. Introduction

Membrane proteins serve many critical roles in the cell including the transmission of information from the external environment to the inside of the cell. They sense the external environment by binding ligands that act as agonists, inverse agonists, antagonists, allosteric

agents, or substrates. The properties of ligands are diverse and can range from ions to small molecules, peptides, or proteins. The nature of interactions between ligands and membrane proteins and the impact that ligand binding has on membrane protein structure are areas that still require more detailed insight. Atomic force microscopy (AFM) is a technique with many different applications in biology and can be used to detect details about single molecules with a spatial resolution on the nanometer scale [1–3]. This methodological platform offers several advantages over more traditional approaches and overcomes some of the barriers in the study of membrane proteins to obtain high-resolution structural and molecular information about the native system.

The study of membrane proteins often involves procedures and manipulations that move the system away from its native condition. Membrane proteins are highly hydrophobic and are natively embedded in a lipid bilayer. Their study is often not fully amenable to traditional methods used to study soluble proteins since the presence of the membrane often interferes with such methods. To circumvent these problems, membrane proteins are extracted from their native membranes using a detergent that maintains protein functionality. Biological membranes play significant roles in protein structure and function and, therefore, it may be questionable as to whether information obtained from extracted membrane proteins accurately reflects the protein under native conditions. Additionally, membrane proteins are often labeled (e.g., fluorescent tags or a staining agent) to facilitate their detection, which can also take the system away from its native condition.

AFM does not require the labeling of proteins and allows for the study of membrane proteins within the context of a lipid bilayer and in a physiological buffer [4–6]. Thus, native properties of membrane proteins can be studied since the conditions these proteins are normally exposed to can be maintained during AFM. In this review, we discuss some of the applications of AFM to study membrane proteins and their interactions with ligands under physiologically relevant conditions and present some examples that illustrate the applications discussed.

2. Atomic force microscopy

AFM was first introduced in 1986 [7]. It was created to overcome the limitations of a related scanning probe microscopy method, scanning tunneling microscopy (STM), which was introduced a few years earlier [8]. Both methods were initially used to image surfaces with atomic resolution. In the case of STM, atomic resolution of surfaces is obtained by monitoring a tunneling current between a sharp probe and a sample surface. Thus, only conductive materials can be investigated. In contrast, atomic resolution of samples is attained in AFM by monitoring small forces applied over a surface using a sharp probe mounted on a flexible cantilever, which acts as a spring and, therefore, the method can be applied to unprocessed biological material. AFM was applied to biological samples in an aqueous environment shortly after its introduction [9,10]. Since the introduction of AFM, this multifunctional technique has found numerous applications in biology and has opened the door for unique inquiries into the structure and function of biomolecules [11,12].

The basic components of an atomic force microscope include a piezoelectric scanner, flexible cantilever containing a sharp probe, laser, photodiode detector, and feedback electronics (Fig. 1A). AFM is based on a simple principle whereby the movements of a flexible cantilever containing an atomically sharp probe are monitored. The movements of the flexible cantilever can be monitored by changes in laser deflection off of a reflective surface on the backside of the cantilever. A photodiode detector detects the changes in deflection of the laser. In many commercial systems, the sample sits on the piezoelectric scanner (e.g., Fig. 1A), which can move in all three dimensions by applying voltage to the piezoelectric material, while the cantilever remains in a fixed position. In other systems, the piezoelectric scanner is attached to the AFM cantilever holder to directly control the movement of the cantilever while the sample remains stationary. This basic set-up allows for both high-resolution imaging and probing of the molecular interactions of biological samples. Thus, the capabilities of AFM extend beyond typical image-based microscopy methods.

One of the most important aspects in the application of AFM to study biological materials is sample preparation. Biological samples must be prepared suitably for the specific AFM application and must be immobilized on a solid substrate (reviewed in [13,14]). The most common substrates used to immobilize membrane protein samples include mica, highly ordered pyrolytic graphite (HOPG), and glass (reviewed in [15,16]). Mica and HOPG are particularly useful for applications that require a clean atomically flat surface. Mica exposes a negatively charged surface while HOPG exposes a hydrophobic surface for samples to adsorb on. Glass substrates can be chemically treated and useful for the attachment of live cells. Table 1 lists the types of membrane protein preparations that are suitable for the different AFM applications discussed here.

3. Imaging membrane proteins and ligands by AFM

3.1. AFM imaging

Membrane proteins present several challenges in their study by high-resolution structural methods as discussed earlier. In addition

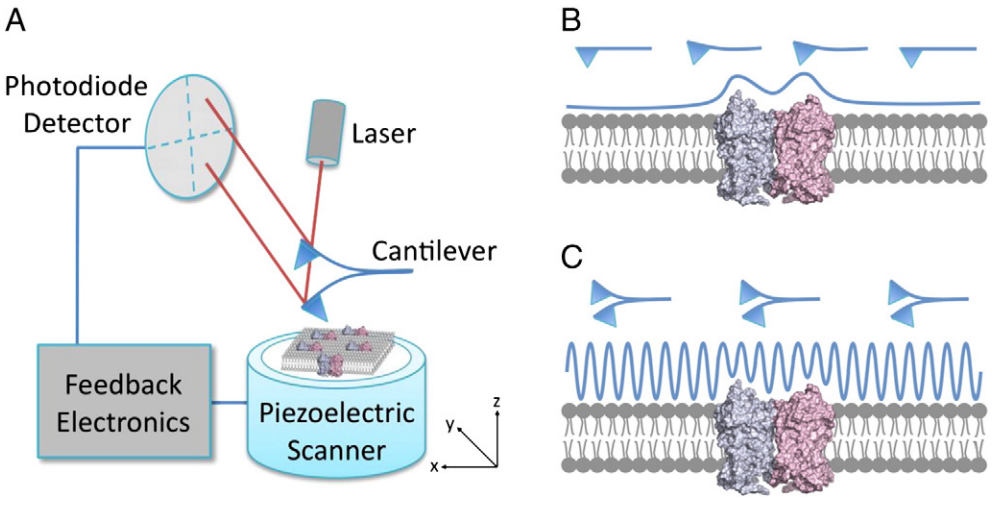

Fig. 1. AFM overview. (A) Components of an atomic force microscope. (B) Contact mode imaging. (C) Tapping mode or intermittent contact mode imaging.

Table 1
Examples of membrane protein–ligand interactions studied using AFM.

Membrane protein (species)	Preparation	Ligand	Membrane protein type, secondary structure	Reference
Imaging studies				
Integrin $\alpha_{IIb}\beta_3$ (human)	Reconstituted lipid bilayer	Fibrinogen	Adhesion protein, single α-helix	[27]
Bacteriorhodopsin (*Halobacterium salinarum*)	Purple membrane	Photon	Transporter, multiple α-helices	[45]
Connexin 26 (rat)	2D crystal in plaques	Ca^{2+}, H^+	Channel, multiple α-helices	[109,110]
KirBac3.1 (*Magnetospirillum magnetotacticum*)	2D crystal in reconstituted lipid bilayer	Mg^{2+}	Channel, multiple α-helices	[111]
MlotiK1 (*Mesorhizobium loti*)	Densely packed in reconstituted lipid bilayer	cAMP	Channel, multiple α-helices	[39]
OmpF (*Escherichia coli*)	2D crystal in reconstituted lipid bilayer	H^+	Channel, β-barrel	[112]
OmpG (*Escherichia. coli*)	2D crystal in reconstituted lipid bilayer	H^+	Channel, β-barrel	[113]
$P2X_4$ receptor (rat)	Reconstituted lipid bilayer	ATP	Channel, multiple α-helices	[114]
Force spectroscopy studies: dissociation of protein–ligand complexes				
Integrins $\alpha_V\beta_3$ and $\alpha_5\beta_1$ (rat)	Osteoclasts	GRGDSP, GRGESP, GRADSP, osteopontin, echistatin	Adhesion protein, single α-helix	[115]
SK channel (rat)	HEK293 cells, hippocampal pyrimidal neurons	Apamin	Channel, multiple α-helices	[116]
CD44 (human)	Human colon cancer cells, reconstituted lipid bilayer	Fibrinogen, P-selectin	Adhesion protein, single α-helix	[117]
LFA-1 (mouse)	3A9 cells	ICAM-1	Adhesion protein, single α-helix	[74]
LHRH receptor (human)	Hela cells	LHRH, LHRH-PE40	GPCR, multiple α-helices	[72]
Mam2 (*Schizosaccharomyces pombe*)	*Schizosaccharomyces pombe*	P factor pheromone	GPCR, multiple α-helices	[118]
Na^+/glucose cotransporter (rabbit)	Brush border membranes, CHO cells	Phlorizin, D-glucose, 1-thio-β-D-glucose	Transporter, multiple α-helices	[119–121]
Serotonin transporter (human)	CHO cells	MFZ2-12	Transporter, multiple α-helices	[67]
TGF-β receptor (human)	HEK293 cells	TGF-β1	Kinase receptor, single α-helix	[122]
Force spectroscopy studies: mechanical protein unfolding				
Aac3p (*Saccharomyces cerevisiae*)	2D crystal in reconstituted lipid bilayer	Atractyloside, carboxy-atractyloside	Transporter, multiple α-helices	[123]
β_2 adrenergic receptor (human)	Reconstituted lipid bilayer	BI, THRX, adrenalin, carazolol, alprenolol	GPCR, multiple α-helices	[93]
BetP (*Corynebacterium glutamicum*)	Reconstituted lipid bilayer	K^+	Transporter, multiple α-helices	[124]
MjNhaP1 (*Methanococcus jannaschii*)	2D crystal in reconstituted lipid bilayer	Na^+	Transporter, multiple α-helices	[125]
NhaA (*Escherichia coli*)	2D crystal in reconstituted lipid bilayer	Na^+, 2-aminoperimidine	Transporter, multiple α-helices	[85,86,126]
OmpG (*Escherichia coli*)	2D crystal in reconstituted lipid bilayer	H^+	Channel, β-barrel	[127,128]
Rhodopsin (mouse)	Rod outer segment disc membranes	11-cis-retinal	GPCR, multiple α-helices	[92]
SteT (*Bacillus subtilis*)	Reconstituted lipid bilayer	L-serine, L-threonine	Transporter, multiple α-helices	[129]

to these challenges, structure determination of full-length multi-domain membrane proteins is often difficult due to their large size or intrinsic flexibility. Thus, structural characterization of multi-domain membrane proteins is often achieved by investigating domains separately, which may not accurately represent the structure of the full-length protein. Moreover, most high-resolution structural methods are not compatible with biological membranes, a challenge that must be overcome since the lipid bilayer is essential for determining native conformations of membrane proteins (e.g., [17–19]). AFM imaging is a high-resolution structural method that overcomes these challenges and allows for the visualization of single protein molecules under physiological conditions.

In AFM imaging, the AFM probe is raster-scanned over the surface of a biological sample to generate a topographical image based on the vertical movements of the cantilever as monitored during the scan. A high signal-to-noise ratio is achievable with AFM, thereby allowing for high-resolution imaging capable of resolving single molecules [20]. Several imaging modes are available in AFM which provide information about the surface properties of materials as experienced by the touch of the AFM probe. The most frequently used AFM imaging modes in biology include contact mode and tapping or intermittent contact mode (reviewed in [21–23]). Both modes are based on the principle of maintaining constant probe force on the sample. The most commonly used modes in biology are overviewed here.

In contact mode [7], the AFM probe maintains constant contact with the sample surface throughout the duration of the scan and the deflection of the cantilever is monitored (Fig. 1B). The feedback electronics adjust the vertical position of the piezoelectric scanner to maintain a constant laser deflection off of the cantilever at a predetermined set-point value, thereby maintaining constant force on the sample. The adjustment in the vertical position required to maintain a constant deflection is recorded and used to generate a topographical image of the sample.

In tapping mode [24], the cantilever is oscillated so that the probe only intermittently contacts the sample. Thus, tapping mode is more suitable for softer or loosely adsorbed samples that can be damaged or deformed by the lateral shear forces present in contact mode imaging. The amplitude of the cantilever's oscillations changes as the height of the sample changes (Fig. 1C). The oscillation amplitude is monitored and the feedback electronics adjust the vertical position of the piezoelectric scanner to maintain a constant amplitude and, therefore, constant applied force. As in contact mode, the adjustments in vertical position of the piezoelectric scanner are recorded and the information used to generate a topographical image. Additionally, the oscillation phase can be monitored [25,26]. Changes in the mechanical properties of the sample, such as friction, adhesion, and stiffness [21,22], will change the phase of the cantilever's oscillations. Phase changes in the cantilever's oscillations can be monitored simultaneously with amplitude changes; therefore, topographical images and phase images can be obtained in the same scan.

3.2. Visualizing single membrane protein–ligand complexes: Integrin $\alpha_{IIb}\beta_3$

Single protein–ligand complexes can be resolved by AFM imaging when the ligand has sufficient size within the detectable resolution limits and binds the membrane protein on an exposed surface that can be tracked by the AFM probe. An example in which AFM imaging was used to resolve single protein–ligand complexes is given in a study investigating the interaction between the platelet integrin $\alpha_{IIb}\beta_3$ and its ligand fibrinogen [27]. Integrin $\alpha_{IIb}\beta_3$ belongs to the integrin superfamily of adhesion proteins and is involved in platelet adhesion, aggregation, and signaling [28,29]. Integrins are heterodimers with each subunit of the dimer containing a single transmembrane domain that anchors the protein in the lipid bilayer and an extracellular domain that binds the ligand. Currently, there is no structure available for a full-length integrin molecule. Structures are only available for the transmembrane domain alone, extracellular domain alone, or short cytoplasmic region alone [30–32]. Integrin $\alpha_{IIb}\beta_3$ binds several different ligands including fibrinogen, a 340 kDa protein exhibiting a trinodal architecture [33,34].

Purified integrin $\alpha_{IIb}\beta_3$ reconstituted into an artificial lipid bilayer was imaged in buffer solution using tapping mode AFM [27]. The structures of both integrin and fibrinogen under physiological conditions exhibit different conformations and dimensions compared to those observed using electron microscopy, where samples are in a dehydrated state [35,36]. Thus, the environmental context of macromolecules is an essential consideration when determining structure and AFM provides the opportunity to investigate membrane proteins and their interactions with ligands within the native context of a lipid bilayer and physiological buffer solution.

Topographical images of integrin $\alpha_{IIb}\beta_3$ embedded in a lipid bilayer incubated with fibrinogen allow resolution of single integrin–fibrinogen complexes (Fig. 2A). Phase images, which are generated based on differences in mechanical properties of the sample surface rather than topography, provide an even clearer picture of fibrinogen bound to its receptor (Fig. 2B). Phase images of integrin $\alpha_{IIb}\beta_3$ alone in the absence of fibrinogen do not reveal distinguishable features. Thus, binding of fibrinogen to integrin $\alpha_{IIb}\beta_3$ results in significant differences in mechanical properties in the region where the protein–ligand complex forms compared to the surrounding lipid bilayer.

High-magnification topographical images of integrin–fibrinogen complexes reveal the trinodal structure of fibrinogen, with each node exhibiting a different height in a cross-sectional line scan (Fig. 2C). Visualizing individual integrin–fibrinogen complexes revealed that fibrinogen could adopt several different conformations when bound to integrin and can bind two integrin molecules simultaneously (Fig. 2C–F). Thus, AFM is a high-resolution method that produces images of single membrane protein–ligand complexes under physiological conditions and reveals conformational variability of individual complexes.

3.3. Observing conformational changes promoted by ligands: MlotiK1 potassium channel

The highest resolution of membrane proteins is possible when proteins are densely packed in a lipid bilayer, sometimes forming 2D crystals, and imaged by contact mode AFM. These conditions allow for a lateral resolution of less than 1 nm; therefore, substructural features of proteins can be resolved [37,38]. Several different types of membrane proteins have been investigated and conformational changes detected upon binding ligands such as protons, Ca^{2+}, and small molecules (Table 1). Moreover, the reversible changes in ligand-promoted conformations can be tracked for single protein molecules. An example illustrating the conformational changes observable by AFM is provided in a study on the MlotiK1 potassium channel [39].

MlotiK1 is a prokaryotic potassium channel from *Mesorhizobium loti* [40]. This protein is a member of the cyclic nucleotide-regulated ion channel family and exhibits a characteristic tetrameric structure in which each subunit consists of 6 transmembrane α-helices and a cytoplasmic cyclic nucleotide-binding domain that binds cAMP or cGMP [41,42]. AFM facilitated the structural characterization of full-length MlotiK1 in the native environment of a lipid bilayer and under buffer conditions with minimal perturbations [39]. MlotiK1 was reconstituted at high density in a lipid bilayer and imaged by contact mode AFM to reveal the topography of the cytoplasmic nucleotide-binding domain, which protrudes out of the membrane (Fig. 3).

Two different conformational states were detected using AFM. When MlotiK1 was bound to cAMP, the cytoplasmic nucleotide-binding domain exhibited a symmetric arrangement of 4 subunits forming a central pore (Fig. 3A–C). The high-affinity binding of cAMP to MlotiK1 precluded the ability to visualize the ligand-free

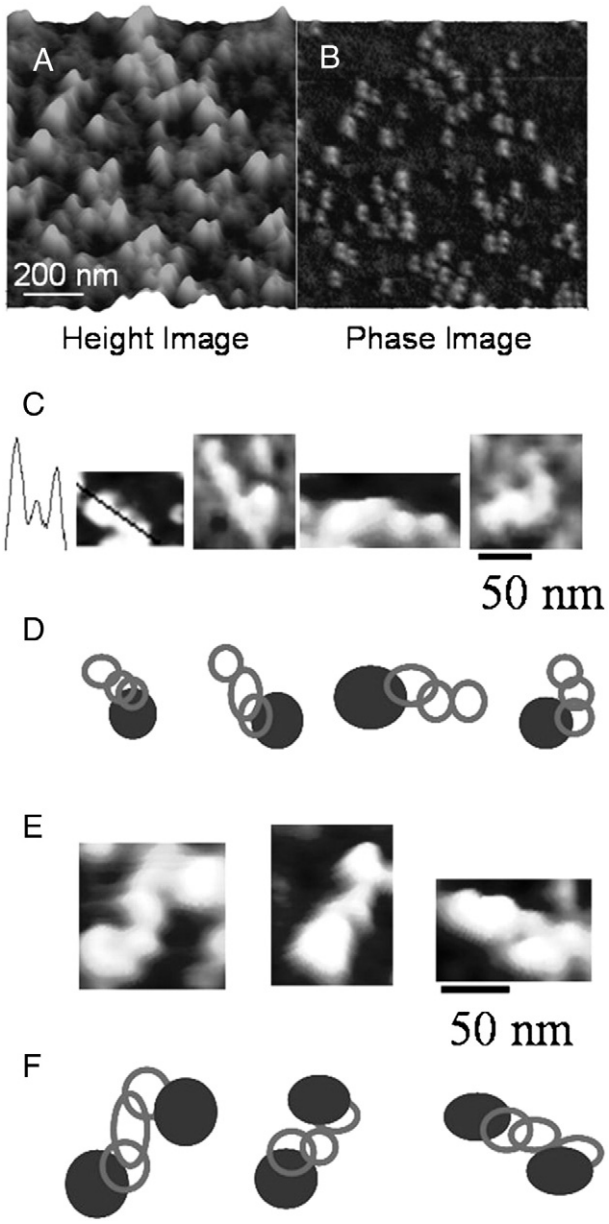

Fig. 2. AFM imaging of integrin $\alpha_{IIb}\beta_3$–fibrinogen complexes. (A) Tapping mode imaging was used to visualize single fibrinogen molecules bound to the integrin $\alpha_{IIb}\beta_3$ in a reconstituted lipid bilayer. Topographical features represent fibrinogen bound to integrin $\alpha_{IIb}\beta_3$. (B) Binding of fibrinogen to the integrin $\alpha_{IIb}\beta_3$ alters the mechanical properties of the sample surface, which is revealed in the phase image. In the absence of fibrinogen, phase images do not reveal any distinguishable features. (C–F) High-magnification tapping mode AFM images and cartoon representation of integrin $\alpha_{IIb}\beta_3$–fibrinogen complexes. A cross-sectional line scan of a feature in AFM images corresponding to fibrinogen displays a topography expected for a trinodal structure (C). A single fibrinogen molecule can bind a single integrin $\alpha_{IIb}\beta_3$ (C, D) or two integrin $\alpha_{IIb}\beta_3$ molecules (E, F). Visualizing single complexes reveals the different conformations fibrinogen adopts when bound to integrin $\alpha_{IIb}\beta_3$. Cartoon representation of integrin $\alpha_{IIb}\beta_3$–fibrinogen complexes is based on AFM images (D, F). Filled ellipses represent integrin $\alpha_{IIb}\beta_3$ and empty ellipses represent the trinodal fibrinogen.
The figure is reprinted with permission from [27]. Copyright (2005) American Chemical Society.

channel. Thus, an R348A mutant with reduced cAMP affinity was used to characterize the ligand-free state of the channel. The cAMP-bound form exhibited a conformation identical to the wild-type channel. However, the ligand-free channel exhibited a significant conformational change in the cytoplasmic ligand-binding domain, which no longer displayed a central pore or distinguishable features (Fig. 3D–F). This conformational change was fully reversible upon reintroduction of

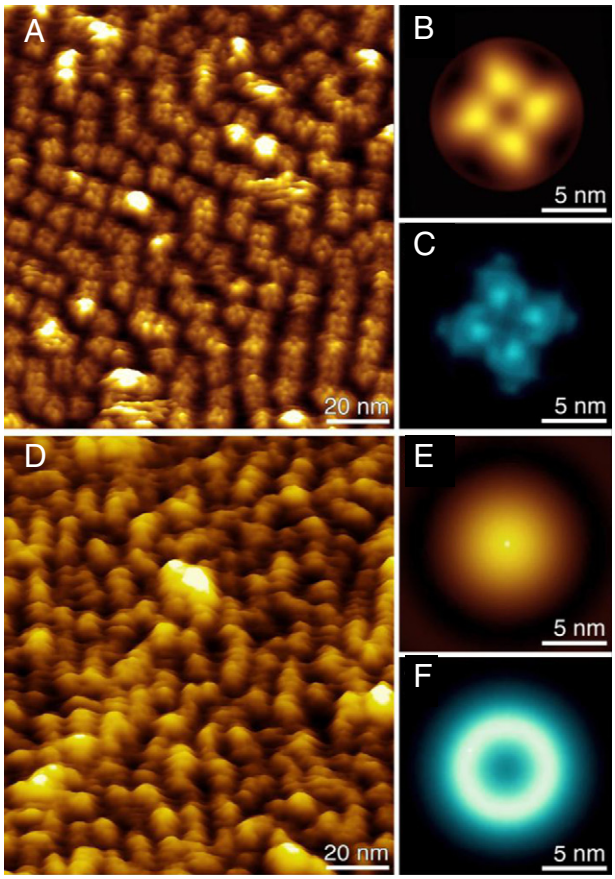

Fig. 3. AFM imaging of ligand-promoted conformational changes in the MlotiK1 potassium channel. (A) High-resolution contact mode AFM imaging reveals the arrangement of single R348A mutant MlotiK1 potassium channels in a reconstituted lipid bilayer in the presence (A–C) or absence (D–F) of the ligand cAMP. Single MlotiK1 molecules resolved in AFM images were used to generate correlation-averaged cAMP-bound (B) and cAMP-free (E) structures. Standard deviation maps were generated that revealed the level of variability in structures of single MlotiK1 molecules used to generate correlation-averaged structures (C, F).
The figure is reprinted with permission from [39] and the National Academy of Sciences, USA.

cAMP. The lack of distinguishable features is suggestive of a conformational state that has greater flexibility or conformational variability compared to the cAMP-bound state [39]. The ability to monitor individual MlotiK1 channels revealed that at subsaturating concentrations of cAMP, only a fraction of the channels exhibited the ligand-free state [39]. This example, along with others listed in Table 1, demonstrates the utility of AFM to visualize conformational changes of membrane proteins promoted by ligands under the native conditions of a lipid bilayer, buffer solution, and ambient temperatures. Moreover, individual protein behavior can be monitored and followed over time and under different conditions.

3.4. High-speed AFM reveals dynamic behavior of single membrane protein molecules: Bacteriorhodopsin

A limitation of conventional AFM is the slow scan rate by the AFM probe necessary to obtain high-resolution images, often in the minute range. The creation of smaller cantilevers and improved instrumentation has led to the development of high-speed AFM, which allows for faster scan rates and the acquisition of high-resolution images in as little as 40 ms [43,44]. The faster image acquisition times in high-speed AFM open the door to tracking biological processes in real-time. We discuss here an example where high-speed AFM was

applied to reveal the dynamics of individual membrane proteins in response to a ligand [45].

Bacteriorhodopsin is a light-driven proton pump found in the purple membrane of *Halobacterium salinarum* and has long served as a model to help understand the structure of membrane proteins [46]. In native purple membrane, bacteriorhodopsin forms trimers that adopt a crystalline arrangement (Fig. 4A). This bacterial proton pump is activated by light via isomerization of all-*trans*-retinal, which is covalently linked to the protein and maintains the inactive basal state. The active state facilitates the proton pumping function and eventually decays back to the inactive basal state [46,47].

High-speed AFM facilitated the real-time monitoring of conformational changes occurring in single bacteriorhodopsin monomers in response to light [45]. A D96N bacteriorhodopsin mutant in the purple membrane of *Halobacterium salinarum* was used in the high-speed AFM studies since it has a 1000-fold slower photocycle (~10 s) compared to wild-type bacteriorhodopsin but retains native function, thereby allowing the detection of conformational changes accompanying light-activation and decay. Activation of bacteriorhodopsin resulted in significant conformational changes of each bacteriorhodopsin monomer within 1 s of light exposure (Fig. 4A and B). Bacteriorhodopsin monomers reverted back to the basal-state conformation in the dark.

The time course was determined for a bacteriorhodopsin monomer to achieve the active-state conformation after illumination of samples and for the decay of this active-state conformation back to the basal-state conformation. Different lighting intensities were used to control the number of bacteriorhodopsin monomers activated and allow for bacteriorhodopsin monomers to be activated at different time points after illumination. The decay rate of the active-state conformation was dependent on whether the activated bacteriorhodopsin monomer in one trimeric complex was in contact with an activated bacteriorhodopsin monomer in an adjacent trimeric complex (Fig. 4C). Under conditions where a single bacteriorhodopsin was activated and not in contact with another activated monomer in adjacent trimers (Fig. 4C, left panel), the active-state conformation decayed exponentially with a time constant of 7.3 s. Under conditions where activated monomers were in contact with other activated monomers in adjacent bacteriorhodopsin trimers, the active-state conformation of the monomer activated last among monomers in adjacent trimers decayed exponentially with a faster time constant of 2 s (Fig. 4C, middle panel). In contrast, monomers activated first among monomers in adjacent trimers do not display an exponential decay of the active-state conformation and this process in those molecules is much slower (Fig. 4C, right panel). Thus, cooperative effects are revealed in the decay rates of the active-state conformation of bacteriorhodopsin when individual protein behaviors are monitored in AFM images. Interestingly, these cooperative effects are not apparent when the active-state conformation decay of all bacteriorhodopsin molecules is analyzed together as would occur in ensemble approaches, thereby highlighting the power of the single-molecule detection capabilities of AFM.

4. Probing single membrane protein–ligand interactions by AFM

4.1. Force spectroscopy: Dissociation of single membrane protein–ligand complexes by force

In addition to providing high-resolution topographical images of sample surfaces, AFM can be used to perform single-molecule force spectroscopy (SMFS) [48–50]. In SMFS, the AFM probe is used to break chemical bonds formed in biological molecules by the application of force using the energy stored in the flexed cantilever. The

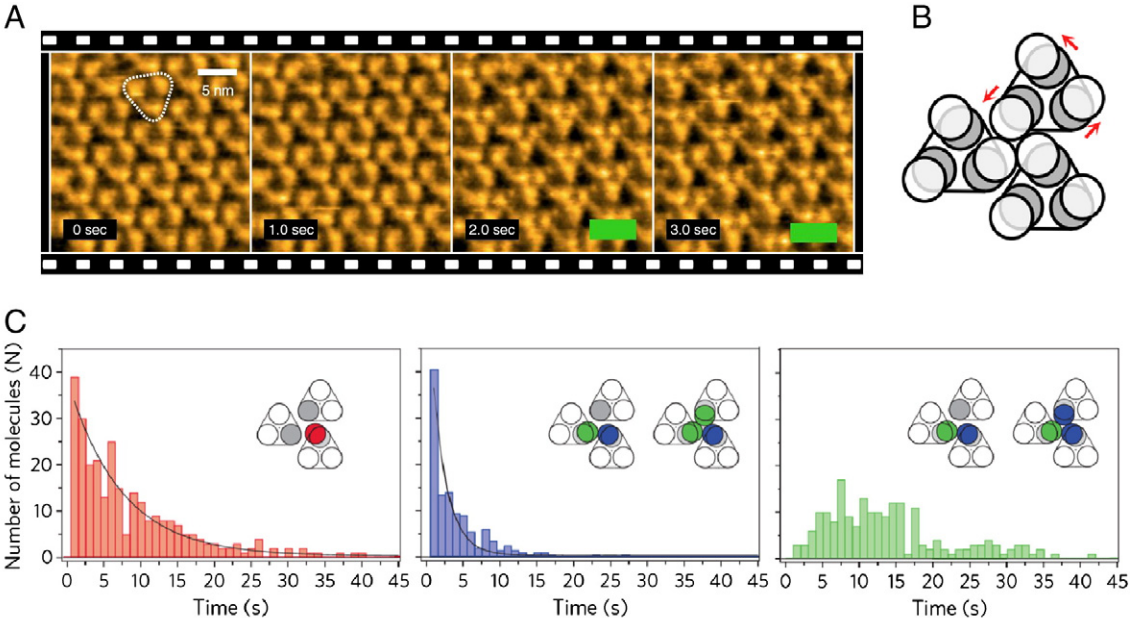

Fig. 4. Dynamics of bacteriorhodopsin revealed by high-speed AFM. (A) High-speed AFM images of D96N mutant bacteriorhodopsin in purple membrane were obtained by tapping mode at a 1 frame per second acquisition speed. Images were collected of the inactive basal state (0–1 s frames) and after light activation (2–3 s frames). A bacteriorhodopsin trimer is outlined in the first frame. (B) A cartoon depiction of bacteriorhodopsin monomers arranged in trimeric complexes in the inactive basal state (gray circles) and the photoactivated state (white circles). Red arrows indicate the direction of conformational changes occurring in each bacteriorhodopsin monomer observed in AFM images. (C) Histograms of decay times for single activated bacteriorhodopsin monomers to revert back to the inactive basal-state conformation as determined from high-speed AFM images. Histograms of decay times are shown for situations where an activated bacteriorhodopsin monomer (red circle) in one trimer does not contact other activated bacteriorhodopsin monomers (gray circles) in adjacent trimers (left panel) or where an activated bacteriorhodopsin monomer in one trimer does make contact with other activated bacteriorhodopsin monomers in adjacent trimers (middle and right panels). For the latter situation, bacteriorhodopsin monomers achieving the active-state conformation first after illumination are shown as green circles and bacteriorhodopsin monomers achieving the active-state conformation last are shown as blue circles. Histograms of decay times are shown for bacteriorhodopsin monomers activated last (blue circles, middle panel) and bacteriorhodopsin monomers activated first (green circles, right panel).
The figure is adapted with permission from [45] and Nature Publishing Group.

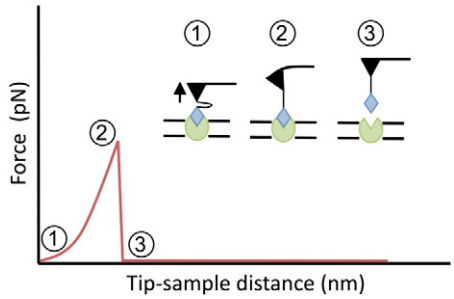

Fig. 5. Probing single protein–ligand interactions by force spectroscopy. A F–D curve recording events that occur during the rupture of chemical bonds between a ligand (blue) functionalized to the AFM probe and a membrane protein (green) is shown. Different parts of the F–D curve are numbered and the corresponding action occurring during the SMFS experiment is shown.

ability to determine the forces, in the pN range, required to rupture chemical bonds allows SMFS to be used to investigate various types of molecular interactions, including those occurring between a protein and ligand and those stabilizing protein structure. SMFS can also be performed using alternate platforms such as optical and magnetic tweezers [51,52].

Functionalization of the AFM probe allows it to be used as bait to probe single protein–ligand interactions. The first studies probing protein–ligand interactions by AFM investigated the adhesive forces involved in the interaction between avidin/streptavidin and biotin [53–55]. A variety of functionalization chemistries have been characterized to attach either a ligand or protein to the surface of an AFM probe for use in SMFS studies [56,57].

In SMFS studies probing protein–ligand interactions, the functionalized AFM probe is brought into contact with the sample surface to allow binding of the attached molecule to its binding partner (Fig. 5). As the AFM probe is retracted from the sample, the chemical bonds stabilizing the protein–ligand pair are stretched until sufficient force is applied to overcome this interaction. The force applied to the protein–ligand pair can be determined from the magnitude of the cantilever's flex as revealed by the laser deflection and knowledge of the cantilever's spring constant. The process of rupturing bonds involved in a protein–ligand interaction in SMFS is recorded in force–distance (F–D) curves (Fig. 5), where a single peak represents the rupture event and the peak height indicates the magnitude of force required to disrupt the adhesion between the protein and the ligand.

The rupture force of chemical bonds is dynamic and dependent on the loading rate (i.e., retraction velocity multiplied by the effective spring constant) [58]. Thus, the rupture force measured in SMFS at a single retraction velocity is only a relative indicator of the interaction strength between a protein and a ligand. The dependence of the rupture force on the loading rate is most frequently rationalized in terms of the Bell–Evans model [59,60]. The Bell–Evans model describes the effect of force on the energy landscape underlying the interaction between a protein and its ligand, thereby providing mechanistic insights into protein–ligand interactions. To obtain these types of insights, SMFS is conducted at different retraction velocities to collect F–D curves in a procedure often referred to as dynamic SMFS (DFS).

In DFS, the average rupture forces are determined from F–D curves collected at different retraction velocities and plotted against the loading rate in DFS plots (Fig. 6A and B). A linear relationship between the average force and the logarithm of the loading rate is indicative of a single activation energy barrier in the energy landscape that separates the bound from unbound protein–ligand complex (e.g., Fig. 6A and C). Utilizing the Bell–Evans model to fit data in DFS plots allows the computation of the following energy landscape parameters: x_β, the distance between the free-energy minimum to the

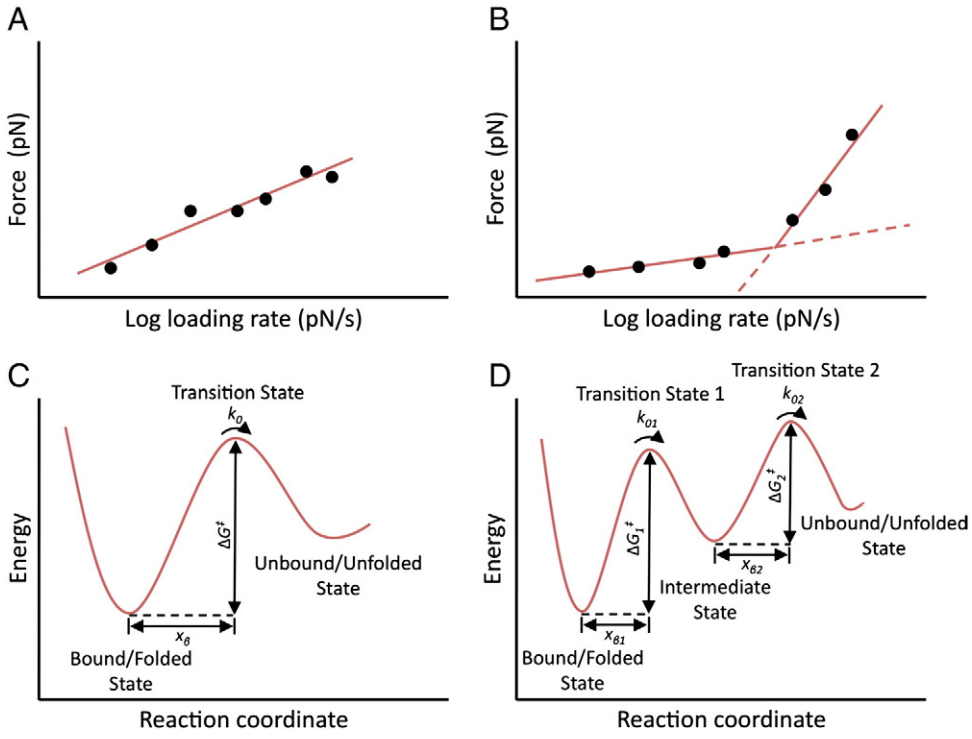

Fig. 6. Dynamic SMFS. SMFS is conducted at different pulling velocities and the average force to disrupt a protein–ligand complex (Fig. 5) or a stable structural segment (Fig. 7) is determined and plotted against the logarithm of the loading rate to generate DFS plots (A, B). The data in these DFS plots can be fitted with a model, such as the Bell–Evans model, to determine parameters describing the energy landscape for protein–ligand dissociation or stable structural segment unfolding (C, D). A linear relationship in DFS plots (A) is indicative of an energy landscape with a single energy barrier (C) and a non-linear relationship in DFS plots (B) is indicative of an energy landscape with multiple energy barriers (D).

transition state barrier, and k_0, the rate constant for protein–ligand dissociation in the absence of applied force. Using the value derived for k_0, the free energy of activation for protein–ligand dissociation, $\Delta G^{\ddagger}$, can be estimated from the Arrhenius equation [61]. Updated models are also actively in development to improve and overcome some of the limitations of the Bell–Evans model to describe DFS data (e.g., [62–64]). A non-linear relationship between force and logarithm of the loading rate, where there are multiple linear regimes (Fig. 6B), is often attributed to multiple free energy activation barriers (Fig. 6D) [65]. In some instances, a non-linear relationship may be indicative of near-equilibrium dissociation [48,66].

SMFS and DFS offer unique opportunities to investigate the dissociation of a membrane protein–ligand complex. The method has high sensitivity and has been used to investigate protein–ligand interactions with equilibrium dissociation constants ranging from fM to μM concentrations [64]. Dissociation rate constants can be determined without considering the complications that exist in more traditional assays due to the reassociation of the protein–ligand complex [64]. Association rate constants can also be computed by determining the probability of interactions between the ligand and the protein by varying the contact time between the functionalized AFM probe and the membrane surface [67]. Determination of the association rate constant is not as straightforward as determining the dissociation rate constant since an accurate estimate of the effective membrane protein concentration must be known. Several different types of protein–ligand interactions have been investigated using SMFS and DFS [68], including those involving membrane proteins (Table 1). Two such studies are described in the following sections.

4.2. Probing single membrane protein–ligand interactions in live cells: Luteinizing hormone-releasing hormone receptor

G protein-coupled receptors (GPCRs) are ubiquitously expressed membrane proteins and form one of the largest classes of therapeutic targets for drugs [69]. Understanding the nature of receptor–ligand interactions is important for the development of new drugs and for revealing insights about the mechanism of receptor action. SMFS provides a method to directly probe the interactions between a GPCR and its ligand in live cells. Luteinizing hormone-releasing hormone (LHRH) receptor is a GPCR that has been found to be overexpressed in several cancer cell lines but absent in healthy human visceral organs [70]. LHRH is a decapeptide hormone and the native agonist for LHRH receptors. LHRH can be fused to peptides with anti-cancer properties and, therefore, has been proposed to be useful in targeting anti-cancer drugs to cancer cells overexpressing LHRH receptors [71]. One proposed anti-cancer drug employs the fusion of LHRH to the toxic *Pseudomonas aeruginosa* exotoxin 40 (PE40) [72]. To characterize the binding properties of LHRH-PE40 to LHRH receptors, SMFS was used to quantify this membrane protein–ligand interaction [72].

SMFS allowed for the investigation of LHRH receptor in the plasma membrane of live Hela cells. AFM probes were functionalized with the ligands, LHRH or LHRH-PE40, via a flexible polyethylene glycol cross-linker, a common approach for probe functionalization [57]. The surface density of attached ligands was adjusted to ensure single receptor–ligand binding events [73]. SMFS was carried out and F–D curves collected, which revealed the specific binding of both ligands to LHRH receptors. DFS plots were generated and revealed a linear relationship between the force and logarithm of loading rate (e.g., Fig. 6A), thereby indicating a single free energy barrier separating the ligand-bound and ligand-free states (e.g., Fig. 6C). Analysis with the Bell–Evans model revealed that both LHRH and LHRH-PE40 have similar dissociation rate constants, indicating that the fusion of PE40 does not interfere with the interaction between LHRH and its receptor. The value computed for x_β provided insight into the potential effect of PE40 on the structure of LHRH. LHRH-PE40 exhibited a smaller x_β than the native LHRH, indicating that the fusion peptide causes LHRH to become more brittle since chemical bonds can be stretched less before overcoming the transition state [72]. Thus, SMFS and DFS can provide insights about the mechanical properties of the ligand itself in addition to providing insights about the kinetics and energetics of the protein–ligand interaction.

4.3. Multiple energy barriers in membrane protein–ligand interactions: Leukocyte function-associated antigen-1

Energy landscapes describing the interaction between a membrane protein and its ligand are a useful tool to understand the mechanism by which this interaction occurs. As illustrated in the previous example, protein–ligand interactions can dissociate via a single energy barrier (e.g., Fig. 6C). In some instances, the nature of the interaction between a protein and ligand is more complex and this complexity can be revealed in the energy landscape. An example of a protein–ligand interaction displaying a complex energy landscape is given in a SMFS study investigating the interaction between the integrin leukocyte function-associated antigen-1 (LFA-1) and its ligand intercellular adhesion molecule-1 (ICAM-1) [74], which mediates leukocyte adhesion [75].

A unique AFM probe functionalization scheme was utilized to investigate LFA-1–ICAM-1 interactions [74]. In contrast to many membrane protein–ligand SMFS studies where the AFM-probe is functionalized with the ligand, the AFM probe in this study was functionalized with a 3A9 cell, a T-cell hybridoma cell line expressing LFA-1 at the cell surface. The adhesive properties between LFA-1 in 3A9 cells and ICAM-1, either functionalized in truncated form on a cell culture dish or expressed on the surface of a cell line, were investigated by SMFS. Single protein–ligand interactions were probed by minimizing the contact time and force applied by the functionalized AFM probe.

LFA-1 exhibits a low-affinity state for ICAM-1 in resting leukocytes and a high-affinity state when activated [76]. LFA-1–ICAM-1 interactions were probed both in resting leukocytes and in an activated state promoted by the addition of Mg^{2+}, thereby allowing a study of the low- and high-affinity states of LFA-1. In both states, DFS plots revealed a non-linear relationship between average force and logarithm of the loading rate (e.g., Fig. 6B), suggesting a complex dissociation pathway involving two energy barriers in the energy landscape underlying protein–ligand dissociation (e.g., Fig. 6D). The outer barrier was defined at lower loading rates while the inner barrier was defined at higher loading rates. The inner barrier was similar for both the low- and high-affinity states of LFA-1; therefore, the difference in affinity of the two states is dictated by the outer barrier, which is the rate-limiting step and reveals a 24-fold slower dissociation rate in the high-affinity state compared to the low-affinity state. The structural origin of the inner barrier was suggested to stem from a chelated Mg^{2+} in LFA-1 that interacts with the ligand ICAM-1 because addition of EDTA precluded the detection of the inner barrier in the fast loading rate regime. These results further suggest that the chelated Mg^{2+} is present in both the low- and high-affinity states of LFA-1 and does not contribute to differences in affinity [74]. Taken together, probing the interaction between LFA-1 and ICAM-1 by SMFS and DFS has revealed new insights about the complex interactions between this protein–ligand pair.

5. Detecting ligand-promoted changes in the molecular interactions of membrane proteins by AFM

5.1. Force spectroscopy: Mechanical unfolding of membrane proteins

SMFS can also be utilized to mechanically unfold membrane proteins and probe the molecular interactions formed to stabilize protein structure and facilitate protein function (Fig. 7) [77]. The first membrane protein to be mechanically unfolded by SMFS was bacteriorhodopsin in purple membrane [78]. The mechanical unfolding of bacteriorhodopsin

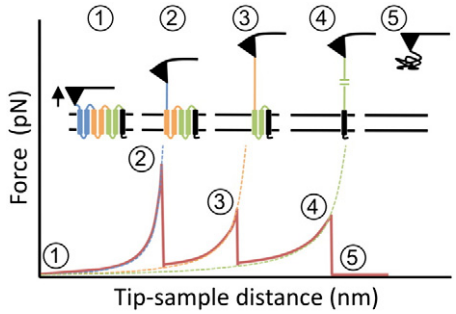

Fig. 7. Mechanical unfolding of membrane proteins by force spectroscopy. A F–D curve recording the mechanical unfolding events of a membrane protein is shown. Different parts of the F–D curve are numbered and the corresponding action occurring during the SMFS experiment is shown. Each peak represents the mechanical unfolding of a stable structural segment (blue, orange, green). Dashed lines represent fitted worm-like chain model curves, which provide an estimate of the contour length.

resulted in the extraction of the protein out of the membrane, as shown by high-resolution AFM images of purple membrane taken before and after mechanical unfolding of bacteriorhodopsin (Fig. 8). An empty space can be seen where the extracted bacteriorhodopsin used to reside (Fig. 8C).

In mechanical unfolding experiments, the AFM probe is pressed into the sample to allow the formation of chemical bonds with the terminal region of the membrane protein that has sufficient strength to facilitate mechanical unfolding. Commercially available silicon nitride AFM probes are most commonly used to allow for non-specific bonds to be formed with side chains of amino acids in the terminal region of the protein. More specific attachments have been achieved using gold-coated AFM probes [78], which form a covalent bond between gold and the sulfhydryl group in the side chain of cysteine residues. Both the non-specific and specific attachments were used to mechanically unfold bacteriorhodopsin out of purple membrane and results were shown to be equivalent [78]. The former type of attachment is more efficient and practical and, therefore, the preferred method.

The bond formed between the AFM probe and terminal region of the membrane protein facilitates the mechanical unfolding of the polypeptide chain as the AFM probe is retracted from the sample surface. During this retraction, the protein is stretched and begins to unfold. The unfolding events of single membrane protein molecules are recorded in F–D curves (Figs. 7 and 8B), which record the amount of force required to overcome stable regions of the protein versus distance between the AFM probe and sample surface. SMFS of membrane proteins reveal F–D curves with multiple peaks, which contrasts with mechanical unfolding of soluble proteins that often unfold in a single step [49,50,79]. Each peak represents the sequential unfolding of a distinct region of the protein that has intrinsic stability to resist unfolding and, therefore, requires external force, originating from energy stored in the flexible cantilever, to overcome the unfolding barrier. Due to the single-molecule nature of the method, variability is observed in the F–D curve peak pattern since the unfolding of a single membrane protein can occur via numerous unfolding pathways. Consistently observed peaks represent the major unfolding events that occur during membrane protein unfolding.

The magnitude of the peaks indicates the amount of force required to unfold a particular region of the protein, thereby providing an estimate of the relative stability of the corresponding region in the protein. Peaks can be analyzed with the worm-like-chain model to compute the contour length [80], which provides an estimate for the length of polypeptide chain stretched between the AFM probe and the membrane surface. Using the contour length, peaks can be assigned to specific regions in the structure of the protein exhibiting stability (Fig. 9), often referred to as stable structural segments [77].

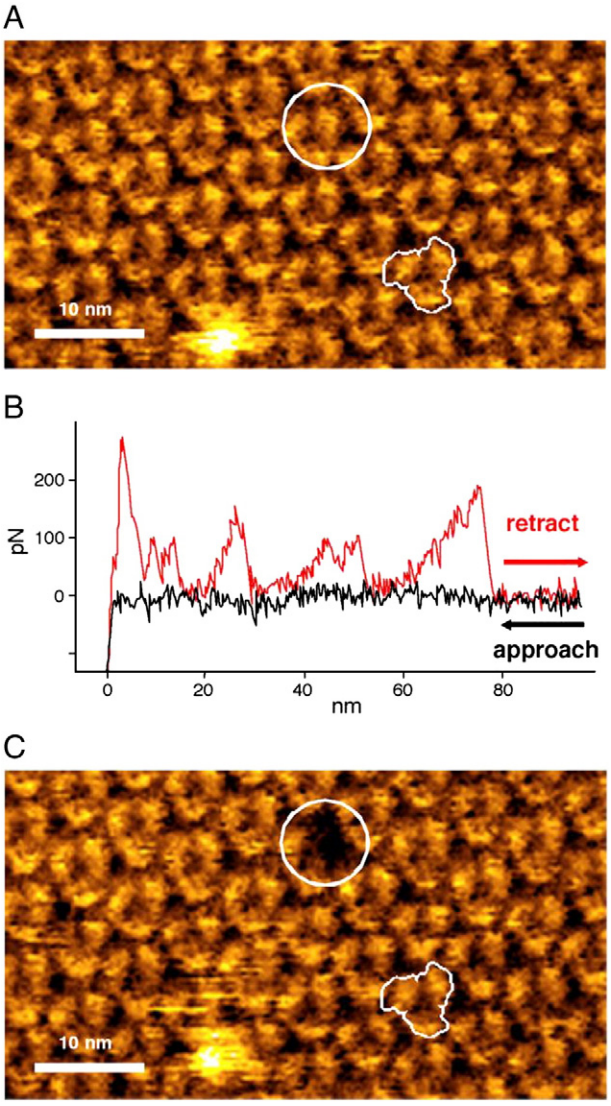

Fig. 8. Mechanical unfolding of single bacteriorhodopsin molecules in purple membrane. (A) Contact mode AFM image of purple membrane before SMFS exhibiting the distinctive trimeric structure of bacteriorhodopsin. (B) F–D curve collected during SMFS representing the mechanical unfolding of a single bacteriorhodopsin molecule (red trace). (C) Contact mode AFM image of purple membrane after collection of the F–D curve revealing the empty space left by the extracted bacteriorhodopsin molecule (highlighted by white circle).
Reprinted with permission from [78] and The American Association for the Advancement of Science.

During a SMFS experiment, stable structural segments unfold sequentially until the entire polypeptide chain is unfolded out of the membrane (Figs. 7 and 8C). Each unfolding event contains information about the nature of molecular interactions in the corresponding region of the protein. The effects of factors, such as mutations [81,82], post-translational modifications [83], lipid bilayer composition [84], or ligands (Table 1), that impact protein structure can be monitored by determining changes in the properties of the molecular interactions involved in forming stable structural segments. The binding of a ligand to a membrane protein can alter the nature of molecular interactions in direct proximity or distal to the ligand-binding pocket. These changes promoted by ligands can manifest in various ways in mechanical unfolding experiments. We discuss here some examples of what can be learned about membrane protein–ligand interactions by mechanically unfolding single membrane protein molecules and list other studies of mechanical unfolding in Table 1.

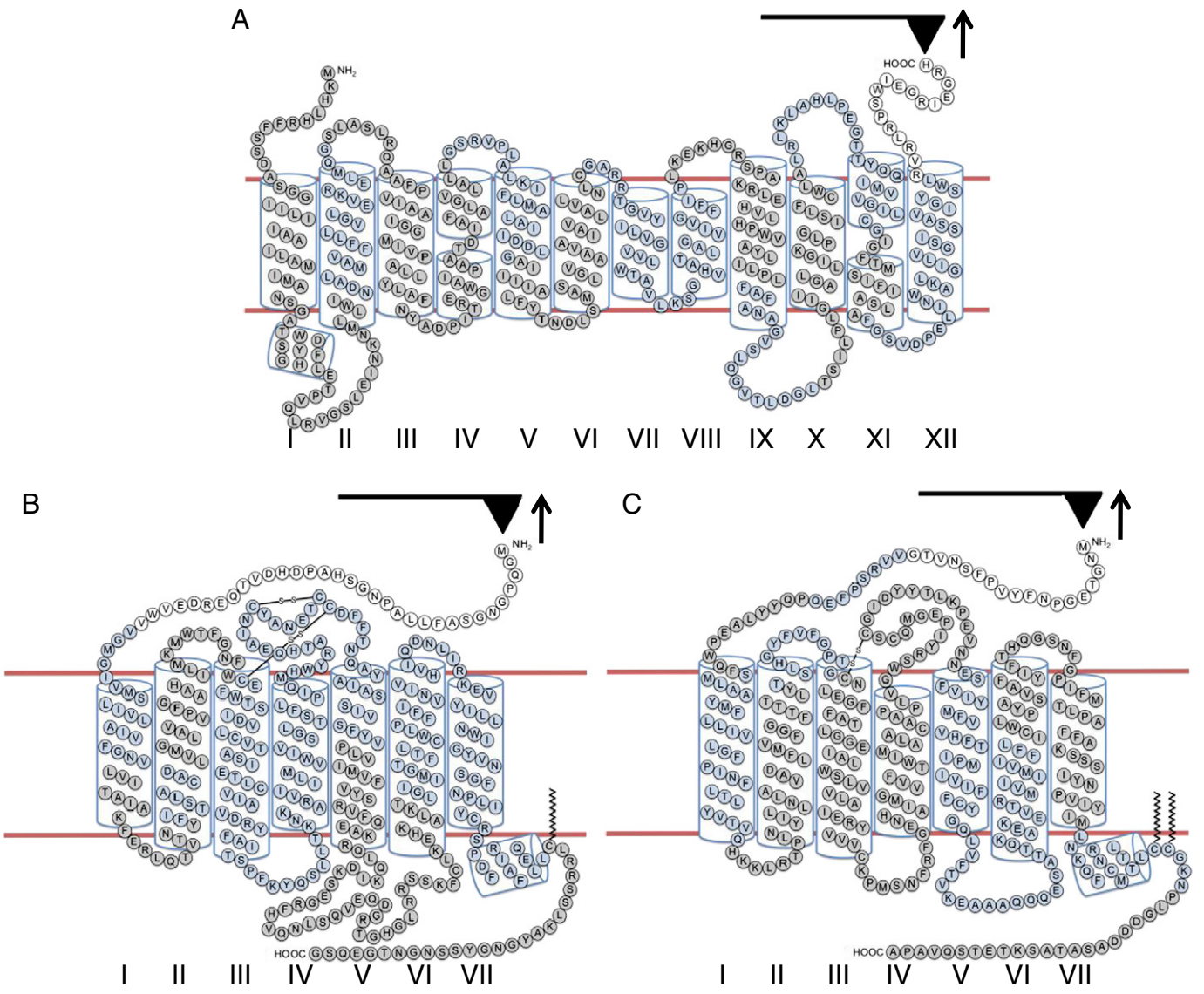

Fig. 9. Stable structural segments of membrane proteins. SMFS reveals the organization of membrane protein structure into stable structural segments, which exhibit stability and require mechanical force to unfold. Stable structural segments of the NhaA Na^+/H^+ antiporter (A), β_2 adrenergic receptor (B), and rhodopsin (C) are shown. Stable structural segment is highlighted on the secondary structures of the membrane proteins alternating in blue and gray coloring. Numbering of transmembrane α-helices is indicated below the secondary structures.

5.2. Localized effects revealed by SMFS: NhaA Na^+/H^+ antiporter

SMFS experiments on NhaA, a bacterial Na^+/H^+ antiporter, have revealed localized effects upon binding of the substrate Na^+ or the inhibitor 2-aminoperimidine [85,86]. NhaA, like other Na^+/H^+ antiporters, plays a critical role in maintaining cellular Na^+ concentrations and pH homeostasis [87]. The activation of this bacterial protein and its ability to bind Na^+ are pH dependent with maximal effects occurring at alkaline pH.

Mechanical unfolding of NhaA in 2D crystals revealed that the protein structure forms 12 stable structural segments (Fig. 9A) [85,86]. The strength of molecular interactions for the stable structural segments was relatively unchanged whether Na^+ was bound or not. An exception was the structural segment containing transmembrane helix V, which required higher forces to unfold and the peak corresponding to this region was observed more frequently when bound to Na^+. As expected, these effects were pH-dependent with maximal effects occurring at neutral-alkaline pH. Consequently, helix V contains amino acid residues that form part of the Na^+ binding pocket [87]. Thus, binding of Na^+ to NhaA resulted in localized effects on molecular interactions stabilizing the region in direct proximity to the ligand-binding pocket.

Binding of the competitive inhibitor 2-aminoperimidine to NhaA resulted in localized effects at a different location compared to those promoted by Na^+ [86]. Binding of the inhibitor was accompanied by increased forces to unfold the stable structural segment harboring transmembrane helix IX, which is in close proximity to the Na^+-binding pocket, while having negligible effects on other stable structural segments including the one affected by Na^+ binding. Thus, inhibitor binding strengthens molecular interactions in helix IX and may also bind in this region. The close proximity of this helix to the Na^+-binding pocket may facilitate competitive inhibition [86].

5.3. Remodeling of the energy landscape promoted by ligands: GPCRs

Mechanical unfolding experiments provide more information than merely localizing stable structural segments and detecting localized effects on the strength of molecular interactions promoted by

ligands. DFS can also be performed in mechanical unfolding studies to determine estimated parameters describing the underlying energy landscape for protein unfolding (Fig. 6), thereby allowing the quantification of the kinetic, energetic, and mechanical properties of stable structural segments of membrane proteins. The energy landscape for protein unfolding, similar to the energy landscape describing other aspects of protein function, has rough surfaces with local energy minima of 4–6 k_BT [88]. Thus, the width of the energy valley of the folded stable structural segment can indicate the conformational variability of a stable structural segment since segments with wider energy valleys can adopt several different conformational substates with similar energetic parameters. The parameter x_β provides an estimate of the width of the energy valley for a folded stable structural segment (Fig. 6C and D) and therefore is an indicator of conformational variability. Mechanical properties of a stable structural segment can also be inferred from DFS-derived parameters by computing a mechanical spring constant, κ, using estimates for $\Delta G^{\ddagger}$ and x_β [89]. Thus, the relative rigidity or flexibility of a stable structural segment can be determined.

Binding of ligands to several membrane proteins has been shown to remodel the unfolding energy landscape, thereby indicating changes in kinetic, energetic and mechanical properties of stabilizing structural segments (Table 1). To illustrate some of these changes, we discuss here the effect of ligands on the stable structural segments formed in GPCRs. Two classical GPCRs have been investigated by DFS, rhodopsin and the β_2 adrenergic receptor. Rhodopsin is the light receptor in the retina that initiates vision. It is covalently bound to the chromophore 11-*cis* retinal, which serves as an inverse agonist locking the receptor in the inactive state. The β_2 adrenergic receptor is a hormone-binding receptor that regulates cardiovascular and pulmonary functions [90]. For both receptors, the free receptor exhibits a low level of constitutive activity.

SMFS and DFS applied to rhodopsin in native rod outer segment disc membranes and purified β_2 adrenergic receptor reconstituted into artificial lipid vesicles revealed the arrangement of stabilizing structural segments in the structures of these GPCRs (Fig. 9B and C) [82,91–93]. In the case of the β_2 adrenergic receptor, agonists, an inverse agonist, and an antagonist all resulted in stable structural segments with increased conformational variability, decreased unfolding rate constants, increased activation energy, and increased flexibility [93]. Each class of ligands, however, changed these properties in a distinct set or subset of stable structural segments, which may underlie the different actions promoted by each class of ligand. Similar to the β_2 adrenergic receptor, the inverse agonist 11-*cis* retinal also resulted in stable structural segments in rhodopsin with increased conformational variability, decreased unfolding rate constants, increased activation energy, and increased flexibility [92]. In contrast to the β_2 adrenergic receptor, the effect of the inverse agonist in rhodopsin exerted these effects on most stable structural segments. Consequently, these effects are lost in a G90D mutant of rhodopsin that is constitutively active when bound to 11-*cis* retinal and causes congenital night blindness [82]. These studies demonstrate the properties of membrane proteins that can be probed by mechanical unfolding experiments to reveal the effect ligands have on the molecular interactions stabilizing membrane protein structure.

6. Concluding remarks

We have presented here some of the unique opportunities AFM provides to probe membrane protein–ligand complexes and the effect ligands have on the structure of membrane proteins under physiologically relevant conditions. AFM provides multiple avenues to investigate biological processes and its applications continue to expand as the technology advances. Improvements in cantilevers and atomic force microscope hardware will increase the speed, resolution, and force sensitivity of the method [2,43,94], thereby providing greater details about the structure and dynamics of membrane proteins. Continued advancement in the integration of AFM with other microscopy and spectroscopy methods will meet the challenges that cannot be overcome by an individual method alone [95,96].

A major advantage of AFM is its ability to detect the structure and behavior of single molecules. Single-molecule methods provide several advantages over more traditional methods including the detection of effects on individual molecules that are often averaged out or masked in ensemble approaches [97]. Proteins are not static structures, but rather dynamic structures that can sample several different states or substates because of thermal fluctuations [98–102]. Many of these states or substates are often undetectable in ensemble approaches since only an average of behaviors is being monitored, yet these undetected effects can play significant roles in protein function [103]. Moreover, functionally important low frequency states or substates may be masked in approaches that detect ensemble averages, but may be apparent in single molecule approaches like AFM [104].

In this review, we have given some examples where single-molecule detection capabilities have provided unique insights about the nature of interactions between a ligand and a membrane protein. However, the single-molecule detection capabilities of AFM have not yet been fully utilized. To better utilize the advantages of single-molecule detection in AFM studies, advances must continue to be forthcoming in the generation and analysis of large data sets. Automated data capture methods and analysis algorithms (e.g., [105–108]) will allow AFM to be developed into a high-throughput method, facilitating the detection and examination of dynamic states and substates that can deviate from ensemble-averaged behaviors. The study of single-molecule behaviors that deviate from ensemble averages will provide a more detailed understanding of the complex issues related to membrane proteins and their interactions with ligands.

Acknowledgements

We would like to thank Christopher A. Siedlecki (The Pennsylvania State University, USA), Daniel J. Müller (ETH Zurich, Switzerland), and Toshio Ando (Kanazawa University, Japan) for providing the images that appeared in Figs. 2, 3, 4, and 8. This work was supported by grants from the National Institutes of Health (R01EY021731) and the Research to Prevent Blindness (Career Development Award). Allison M. Whited was supported by the Visual Sciences Training Program grant from the National Institutes of Health (T32EY007157).

References

[1] D.J. Muller, Y.F. Dufrene, Atomic force microscopy as a multifunctional molecular toolbox in nanobiotechnology, Nat. Nanotechnol. 3 (2008) 261–269.
[2] I. Casuso, F. Rico, S. Scheuring, Biological AFM: where we come from–where we are–where we may go, J. Mol. Recognit. 24 (2011) 406–413.
[3] C.M. Yip, Atomic force microscopy of macromolecular interactions, Curr. Opin. Struct. Biol. 11 (2001) 567–572.
[4] A. Engel, H.E. Gaub, Structure and mechanics of membrane proteins, Annu. Rev. Biochem. 77 (2008) 127–148.
[5] D.J. Muller, AFM: a nanotool in membrane biology, Biochemistry 47 (2008) 7986–7998.
[6] D. Fotiadis, Atomic force microscopy for the study of membrane proteins, Curr. Opin. Biotechnol. 23 (2012) 510–515.
[7] G. Binnig, C.F. Quate, C. Gerber, Atomic force microscope, Phys. Rev. Lett. 56 (1986) 930–933.
[8] G. Binnig, H. Rohrer, C. Gerber, E. Weibel, Tunneling through a controllable vacuum gap, Appl. Phys. Lett. 40 (1982) 178–180.
[9] B. Drake, C.B. Prater, A.L. Weisenhorn, S.A. Gould, T.R. Albrecht, C.F. Quate, D.S. Cannell, H.G. Hansma, P.K. Hansma, Imaging crystals, polymers, and processes in water with the atomic force microscope, Science 243 (1989) 1586–1589.
[10] S.M. Lindsay, L.A. Nagahara, T. Thundat, U. Knipping, R.L. Rill, B. Drake, C.B. Prater, A.L. Weisenhorn, S.A. Gould, P.K. Hansma, STM and AFM images of nucleosome DNA under water, J. Biomol. Struct. Dyn. 7 (1989) 279–287.
[11] C. Gerber, H.P. Lang, How the doors to the nanoworld were opened, Nat. Nanotechnol. 1 (2006) 3–5.

[12] P. Parot, Y.F. Dufrene, P. Hinterdorfer, C. Le Grimellec, D. Navajas, J.L. Pellequer, S. Scheuring, Past, present and future of atomic force microscopy in life sciences and medicine, J. Mol. Recognit. 20 (2007) 418–431.
[13] K. El Kirat, I. Burton, V. Dupres, Y.F. Dufrene, Sample preparation procedures for biological atomic force microscopy, J. Microsc. 218 (2005) 199–207.
[14] D.J. Muller, A. Engel, M. Amrein, Preparation techniques for the observation of native biological systems with the atomic force microscope, Biosens. Bioelectron. 12 (1997) 867–877.
[15] D.J. Muller, A. Engel, Atomic force microscopy and spectroscopy of native membrane proteins, Nat. Protoc. 2 (2007) 2191–2197.
[16] T. Puntheeranurak, I. Neundlinger, R.K. Kinne, P. Hinterdorfer, Single-molecule recognition force spectroscopy of transmembrane transporters on living cells, Nat. Protoc. 6 (2011) 1443–1452.
[17] G.M. Clayton, S.G. Aller, J. Wang, V. Unger, J.H. Morais-Cabral, Combining electron crystallography and X-ray crystallography to study the MlotiK1 cyclic nucleotide-regulated potassium channel, J. Struct. Biol. 167 (2009) 220–226.
[18] H. Zheng, W. Liu, L.Y. Anderson, Q.X. Jiang, Lipid-dependent gating of a voltage-gated potassium channel, Nat. Commun. 2 (2011) 250.
[19] S.Y. Lee, A. Lee, J. Chen, R. MacKinnon, Structure of the KvAP voltage-dependent K^+ channel and its dependence on the lipid membrane, Proc. Natl. Acad. Sci. U. S. A. 102 (2005) 15441–15446.
[20] P. Fechner, T. Boudier, S. Mangenot, S. Jaroslawski, J.N. Sturgis, S. Scheuring, Structural information, resolution, and noise in high-resolution atomic force microscopy topographs, Biophys. J. 96 (2009) 3822–3831.
[21] J.L. Alonso, W.H. Goldmann, Feeling the forces: atomic force microscopy in cell biology, Life Sci. 72 (2003) 2553–2560.
[22] P.T. Frederix, B.W. Hoogenboom, D. Fotiadis, D.J. Muller, A. Engel, Atomic force microscopy of biological samples, MRS Bull. 29 (2004) 449–455.
[23] H.G. Hansma, J.H. Hoh, Biomolecular imaging with the atomic force microscope, Annu. Rev. Biophys. Biomol. Struct. 23 (1994) 115–139.
[24] Q. Zhong, D. Inniss, K. Kjoller, V.B. Elings, Fractured polymer silica fiber surface studied by tapping mode atomic-force microscopy, Surf. Sci. 290 (1993) L688–L692.
[25] S.N. Magonov, V. Elings, M.H. Whangbo, Phase imaging and stiffness in tapping-mode atomic force microscopy, Surf. Sci. 375 (1997) L385–L391.
[26] I. Schmitz, M. Schreiner, G. Friedbacher, M. Grasserbauer, Phase imaging as an extension to tapping mode AFM for the identification of material properties on humidity-sensitive surfaces, Appl. Surf. Sci. 115 (1997) 190–198.
[27] M.A. Hussain, A. Agnihotri, C.A. Siedlecki, AFM imaging of ligand binding to platelet integrin αIIbβ3 receptors reconstituted into planar lipid bilayers, Langmuir 21 (2005) 6979–6986.
[28] N. Kieffer, D.R. Phillips, Platelet membrane glycoproteins: functions in cellular interactions, Annu. Rev. Cell Biol. 6 (1990) 329–357.
[29] R.O. Hynes, Integrins: versatility, modulation, and signaling in cell adhesion, Cell 69 (1992) 11–25.
[30] T.L. Lau, C. Kim, M.H. Ginsberg, T.S. Ulmer, The structure of the integrin αIIbβ3 transmembrane complex explains integrin transmembrane signalling, EMBO J. 28 (2009) 1351–1361.
[31] J.P. Xiong, T. Stehle, B. Diefenbach, R. Zhang, R. Dunker, D.L. Scott, A. Joachimiak, S.L. Goodman, M.A. Arnaout, Crystal structure of the extracellular segment of integrin αVβ3, Science 294 (2001) 339–345.
[32] O. Vinogradova, A. Velyvis, A. Velyviene, B. Hu, T. Haas, E. Plow, J. Qin, A structural mechanism of integrin αIIbβ3 "inside-out" activation as regulated by its cytoplasmic face, Cell 110 (2002) 587–597.
[33] J.W. Weisel, C.V. Stauffacher, E. Bullitt, C. Cohen, A model for fibrinogen: domains and sequence, Science 230 (1985) 1388–1391.
[34] J.M. Kollman, L. Pandi, M.R. Sawaya, M. Riley, R.F. Doolittle, Crystal structure of human fibrinogen, Biochemistry 48 (2009) 3877–3886.
[35] M.A. Hussain, C.A. Siedlecki, The platelet integrin αIIbβ3 imaged by atomic force microscopy on model surfaces, Micron 35 (2004) 565–573.
[36] P.S. Sit, R.E. Marchant, Surface-dependent conformations of human fibrinogen observed by atomic force microscopy under aqueous conditions, Thromb. Haemost. 82 (1999) 1053–1060.
[37] D. Fotiadis, S. Scheuring, S.A. Müller, A. Engel, D.J. Müller, Imaging and manipulation of biological structures with the AFM, Micron 33 (2002) 385–397.
[38] D.M. Czajkowsky, Z. Shao, Submolecular resolution of single macromolecules with atomic force microscopy, FEBS Lett. 430 (1998) 51–54.
[39] S.A. Mari, J. Pessoa, S. Altieri, U. Hensen, L. Thomas, J.H. Morais-Cabral, D.J. Muller, Gating of the MlotiK1 potassium channel involves large rearrangements of the cyclic nucleotide-binding domains, Proc. Natl. Acad. Sci. U. S. A. 108 (2011) 20802–20807.
[40] C.M. Nimigean, T. Shane, C. Miller, A cyclic nucleotide modulated prokaryotic K^+ channel, J. Gen. Physiol. 124 (2004) 203–210.
[41] U.B. Kaupp, R. Seifert, Cyclic nucleotide-gated ion channels, Physiol. Rev. 82 (2002) 769–824.
[42] K.B. Craven, W.N. Zagotta, CNG and HCN channels: two peas, one pod, Annu. Rev. Physiol. 68 (2006) 375–401.
[43] T. Ando, High-speed atomic force microscopy coming of age, Nanotechnology 23 (2012) 062001.
[44] I. Casuso, F. Rico, S. Scheuring, High-speed atomic force microscopy: structure and dynamics of single proteins, Curr. Opin. Chem. Biol. 15 (2011) 704–709.
[45] M. Shibata, H. Yamashita, T. Uchihashi, H. Kandori, T. Ando, High-speed atomic force microscopy shows dynamic molecular processes in photoactivated bacteriorhodopsin, Nat. Nanotechnol. 5 (2010) 208–212.
[46] U. Haupts, J. Tittor, D. Oesterhelt, Closing in on bacteriorhodopsin: progress in understanding the molecule, Annu. Rev. Biophys. Biomol. Struct. 28 (1999) 367–399.
[47] J.K. Lanyi, Bacteriorhodopsin, Annu. Rev. Physiol. 66 (2004) 665–688.
[48] A. Noy, Force spectroscopy 101: how to design, perform, and analyze an AFM-based single molecule force spectroscopy experiment, Curr. Opin. Chem. Biol. 15 (2011) 710–718.
[49] E.M. Puchner, H.E. Gaub, Force and function: probing proteins with AFM-based force spectroscopy, Curr. Opin. Struct. Biol. 19 (2009) 605–614.
[50] M. Rief, H. Grubmuller, Force spectroscopy of single biomolecules, Chemphyschem 3 (2002) 255–261.
[51] K.C. Neuman, A. Nagy, Single-molecule force spectroscopy: optical tweezers, magnetic tweezers and atomic force microscopy, Nat. Methods 5 (2008) 491–505.
[52] C. Bustamante, J.C. Macosko, G.J. Wuite, Grabbing the cat by the tail: manipulating molecules one by one, Nat. Rev. Mol. Cell Biol. 1 (2000) 130–136.
[53] E.L. Florin, V.T. Moy, H.E. Gaub, Adhesion forces between individual ligand–receptor pairs, Science 264 (1994) 415–417.
[54] V.T. Moy, E.L. Florin, H.E. Gaub, Intermolecular forces and energies between ligands and receptors, Science 266 (1994) 257–259.
[55] G.U. Lee, D.A. Kidwell, R.J. Colton, Sensing discrete streptavidin–biotin interactions with atomic force microscopy, Langmuir 10 (1994) 354–357.
[56] R. Barattin, N. Voyer, Chemical modifications of AFM tips for the study of molecular recognition events, Chem. Commun. (Camb.) (2008) 1513–1532.
[57] P. Hinterdorfer, Y.F. Dufrene, Detection and localization of single molecular recognition events using atomic force microscopy, Nat. Methods 3 (2006) 347–355.
[58] E. Evans, Probing the relation between force–lifetime–and chemistry in single molecular bonds, Annu. Rev. Biophys. Biomol. Struct. 30 (2001) 105–128.
[59] E. Evans, K. Ritchie, Dynamic strength of molecular adhesion bonds, Biophys. J. 72 (1997) 1541–1555.
[60] G.I. Bell, Models for the specific adhesion of cells to cells, Science 200 (1978) 618–627.
[61] H. Dietz, M. Rief, Exploring the energy landscape of GFP by single-molecule mechanical experiments, Proc. Natl. Acad. Sci. U. S. A. 101 (2004) 16192–16197.
[62] O.K. Dudko, G. Hummer, A. Szabo, Theory, analysis, and interpretation of single-molecule force spectroscopy experiments, Proc. Natl. Acad. Sci. U. S. A. 105 (2008) 15755–15760.
[63] O.K. Dudko, G. Hummer, A. Szabo, Intrinsic rates and activation free energies from single-molecule pulling experiments, Phys. Rev. Lett. 96 (2006) 108101.
[64] A. Fuhrmann, R. Ros, Single-molecule force spectroscopy: a method for quantitative analysis of ligand–receptor interactions, Nanomedicine 5 (2010) 657–666.
[65] R. Merkel, P. Nassoy, A. Leung, K. Ritchie, E. Evans, Energy landscapes of receptor–ligand bonds explored with dynamic force spectroscopy, Nature 397 (1999) 50–53.
[66] R.W. Friddle, A. Noy, J.J. De Yoreo, Interpreting the widespread nonlinear force spectra of intermolecular bonds, Proc. Natl. Acad. Sci. U. S. A. 109 (2012) 13573–13578.
[67] L. Wildling, C. Rankl, T. Haselgrubler, H.J. Gruber, M. Holy, A.H. Newman, M.F. Zou, R. Zhu, M. Freissmuth, H.H. Sitte, P. Hinterdorfer, Probing binding pocket of serotonin transporter by single molecular force spectroscopy on living cells, J. Biol. Chem. 287 (2012) 105–113.
[68] C.K. Lee, Y.M. Wang, L.S. Huang, S. Lin, Atomic force microscopy: determination of unbinding force, off rate and energy barrier for protein–ligand interaction, Micron 38 (2007) 446–461.
[69] K. Lundstrom, An overview on GPCRs and drug discovery: structure-based drug design and structural biology on GPCRs, Methods Mol. Biol. 552 (2009) 51–66.
[70] S.S. Dharap, T. Minko, Targeted proapoptotic LHRH-BH3 peptide, Pharm. Res. 20 (2003) 889–896.
[71] S.S. Dharap, Y. Wang, P. Chandna, J.J. Khandare, B. Qiu, S. Gunaseelan, P.J. Sinko, S. Stein, A. Farmanfarmaian, T. Minko, Tumor-specific targeting of an anticancer drug delivery system by LHRH peptide, Proc. Natl. Acad. Sci. U. S. A. 102 (2005) 12962–12967.
[72] J. Zhang, G. Wu, C. Song, Y. Li, H. Qiao, P. Zhu, P. Hinterdorfer, B. Zhang, J. Tang, Single molecular recognition force spectroscopy study of a luteinizing hormone-releasing hormone analogue as a carcinoma target drug, J. Phys. Chem. B 116 (2012) 13331–13337.
[73] A. Ebner, L. Wildling, A.S.M. Kamruzzahan, C. Rankl, J. Wruss, C.D. Hahn, M. Holzl, R. Zhu, F. Kienberger, D. Blaas, P. Hinterdorfer, H.J. Gruber, A new, simple method for linking of antibodies to atomic force microscopy tips, Bioconjug. Chem. 18 (2007) 1176–1184.
[74] X. Zhang, E. Wojcikiewicz, V.T. Moy, Force spectroscopy of the leukocyte function-associated antigen-1/intercellular adhesion molecule-1 interaction, Biophys. J. 83 (2002) 2270–2279.
[75] F. Sanchez-Madrid, P. Simon, S. Thompson, T.A. Springer, Mapping of antigenic and functional epitopes on the alpha- and beta-subunits of two related mouse glycoproteins involved in cell interactions, LFA-1 and Mac-1, J. Exp. Med. 158 (1983) 586–602.
[76] M. Stewart, N. Hogg, Regulation of leukocyte integrin function: affinity vs. avidity, J. Cell. Biochem. 61 (1996) 554–561.
[77] A. Kedrov, H. Janovjak, K.T. Sapra, D.J. Muller, Deciphering molecular interactions of native membrane proteins by single-molecule force spectroscopy, Annu. Rev. Biophys. Biomol. Struct. 36 (2007) 233–260.
[78] F. Oesterhelt, D. Oesterhelt, M. Pfeiffer, A. Engel, H.E. Gaub, D.J. Müller, Unfolding pathways of individual bacteriorhodopsins, Science 288 (2000) 143–146.
[79] T.E. Fisher, A.F. Oberhauser, M. Carrion-Vazquez, P.E. Marszalek, J.M. Fernandez, The study of protein mechanics with the atomic force microscope, Trends Biochem. Sci. 24 (1999) 379–384.
[80] C. Bustamante, J.F. Marko, E.D. Siggia, S. Smith, Entropic elasticity of lambda-phage DNA, Science 265 (1994) 1599–1600.
[81] K.T. Sapra, G.P. Balasubramanian, D. Labudde, J.U. Bowie, D.J. Muller, Point mutations in membrane proteins reshape energy landscape and populate different unfolding pathways, J. Mol. Biol. 376 (2008) 1076–1090.

[82] S. Kawamura, A.T. Colozo, L. Ge, D.J. Muller, P.S. Park, Structural, energetic, and mechanical perturbations in rhodopsin mutant that causes congenital stationary night blindness, J. Biol. Chem. 287 (2012) 21826–21835.
[83] P.S. Park, K.T. Sapra, B. Jastrzebska, T. Maeda, A. Maeda, W. Pulawski, M. Kono, J. Lem, R.K. Crouch, S. Filipek, D.J. Muller, K. Palczewski, Modulation of molecular interactions and function by rhodopsin palmitylation, Biochemistry 48 (2009) 4294–4304.
[84] M. Zocher, C. Zhang, S.G. Rasmussen, B.K. Kobilka, D.J. Muller, Cholesterol increases kinetic, energetic, and mechanical stability of the human β2-adrenergic receptor, Proc. Natl. Acad. Sci. U. S. A. 109 (2012) E3463–E3472.
[85] A. Kedrov, M. Krieg, C. Ziegler, W. Kuhlbrandt, D.J. Muller, Locating ligand binding and activation of a single antiporter, EMBO Rep. 6 (2005) 668–674.
[86] A. Kedrov, C. Ziegler, D.J. Muller, Differentiating ligand and inhibitor interactions of a single antiporter, J. Mol. Biol. 362 (2006) 925–932.
[87] E. Padan, The enlightening encounter between structure and function in the NhaA Na^+–H^+ antiporter, Trends Biochem. Sci. 33 (2008) 435–443.
[88] H. Janovjak, H. Knaus, D.J. Muller, Transmembrane helices have rough energy surfaces, J. Am. Chem. Soc. 129 (2007) 246–247.
[89] K.T. Sapra, P.S. Park, K. Palczewski, D.J. Muller, Mechanical properties of bovine rhodopsin and bacteriorhodopsin: possible roles in folding and function, Langmuir 24 (2008) 1330–1337.
[90] G. Milligan, P. Svoboda, C.M. Brown, Why are there so many adrenoceptor subtypes? Biochem. Pharmacol. 48 (1994) 1059–1071.
[91] S. Kawamura, A.T. Colozo, D.J. Muller, P.S. Park, Conservation of molecular interactions stabilizing bovine and mouse rhodopsin, Biochemistry 49 (2010) 10412–10420.
[92] S. Kawamura, M. Gerstung, A.T. Colozo, J. Helenius, A. Maeda, N. Beerenwinkel, P.S. Park, D.J. Muller, Kinetic, energetic, and mechanical differences between dark-state rhodopsin and opsin, Structure 21 (2013) 426–437.
[93] M. Zocher, J.J. Fung, B.K. Kobilka, D.J. Muller, Ligand-specific interactions modulate kinetic, energetic, and mechanical properties of the human β2 adrenergic receptor, Structure 20 (2012) 1391–1402.
[94] M. Leitner, G.E. Fantner, E.J. Fantner, K. Ivanova, T. Ivanov, I. Rangelow, A. Ebner, M. Rangl, J. Tang, P. Hinterdorfer, Increased imaging speed and force sensitivity for bio-applications with small cantilevers using a conventional AFM setup, Micron 43 (2012) 1399–1407.
[95] C.M. Yip, Correlative optical and scanning probe microscopies for mapping interactions at membranes, Methods Mol. Biol. 950 (2013) 439–456.
[96] J.E. Verity, N. Chhabra, K. Sinnathamby, C.M. Yip, Tracking molecular interactions in membranes by simultaneous ATR-FTIR-AFM, Biophys. J. 97 (2009) 1225–1231.
[97] N.G. Walter, C.Y. Huang, A.J. Manzo, M.A. Sobhy, Do-it-yourself guide: how to use the modern single-molecule toolkit, Nat. Methods 5 (2008) 475–489.
[98] P.S. Park, Ensemble of G protein-coupled receptor active states, Curr. Med. Chem. 19 (2012) 1146–1154.
[99] E. Freire, Statistical thermodynamic linkage between conformational and binding equilibria, Adv. Protein Chem. 51 (1998) 255–279.
[100] V.J. Hilser, E.B. Garcia-Moreno, T.G. Oas, G. Kapp, S.T. Whitten, A statistical thermodynamic model of the protein ensemble, Chem. Rev. 106 (2006) 1545–1558.
[101] B. Ma, M. Shatsky, H.J. Wolfson, R. Nussinov, Multiple diverse ligands binding at a single protein site: a matter of pre-existing populations, Protein Sci. 11 (2002) 184–197.
[102] K.A. Dill, H.S. Chan, From Levinthal to pathways to funnels, Nat. Struct. Biol. 4 (1997) 10–19.
[103] M. Vendruscolo, C.M. Dobson, Structural biology. Dynamic visions of enzymatic reactions, Science 313 (2006) 1586–1587.
[104] M. Schlierf, H. Li, J.M. Fernandez, The unfolding kinetics of ubiquitin captured with single-molecule force-clamp techniques, Proc. Natl. Acad. Sci. U. S. A. 101 (2004) 7299–7304.
[105] I. Casuso, S. Scheuring, Automated setpoint adjustment for biological contact mode atomic force microscopy imaging, Nanotechnology 21 (2010) 035104.
[106] J. Struckmeier, R. Wahl, M. Leuschner, J. Nunes, H. Janovjak, U. Geisler, G. Hofmann, T. Jahnke, D.J. Muller, Fully automated single-molecule force spectroscopy for screening applications, Nanotechnology 19 (2008) 384020.
[107] P.D. Bosshart, P.L. Frederix, A. Engel, Reference-free alignment and sorting of single-molecule force spectroscopy data, Biophys. J. 102 (2012) 2202–2211.
[108] P.D. Bosshart, F. Casagrande, P.L. Frederix, M. Ratera, C.A. Bippes, D.J. Muller, M. Palacin, A. Engel, D. Fotiadis, High-throughput single-molecule force spectroscopy for membrane proteins, Nanotechnology 19 (2008) 384014.
[109] D.J. Muller, G.M. Hand, A. Engel, G.E. Sosinsky, Conformational changes in surface structures of isolated connexin 26 gap junctions, EMBO J. 21 (2002) 3598–3607.
[110] J. Yu, C.A. Bippes, G.M. Hand, D.J. Muller, G.E. Sosinsky, Aminosulfonate modulated pH-induced conformational changes in connexin26 hemichannels, J. Biol. Chem. 282 (2007) 8895–8904.
[111] S. Jaroslawski, B. Zadek, F. Ashcroft, C. Venien-Bryan, S. Scheuring, Direct visualization of KirBac3.1 potassium channel gating by atomic force microscopy, J. Mol. Biol. 374 (2007) 500–505.
[112] D.J. Muller, A. Engel, Voltage and pH-induced channel closure of porin OmpF visualized by atomic force microscopy, J. Mol. Biol. 285 (1999) 1347–1351.
[113] S.A. Mari, S. Koster, C.A. Bippes, O. Yildiz, W. Kuhlbrandt, D.J. Muller, pH-induced conformational change of the beta-barrel-forming protein OmpG reconstituted into native *E. coli* lipids, J. Mol. Biol. 396 (2009) 610–616.
[114] Y. Shinozaki, K. Sumitomo, M. Tsuda, S. Koizumi, K. Inoue, K. Torimitsu, Direct observation of ATP-induced conformational changes in single P2X(4) receptors, PLoS Biol. 7 (2009) e1000103.
[115] P.P. Lehenkari, M.A. Horton, Single integrin molecule adhesion forces in intact cells measured by atomic force microscopy, Biochem. Biophys. Res. Commun. 259 (1999) 645–650.
[116] J.L. Maciaszek, H. Soh, R.S. Walikonis, A.V. Tzingounis, G. Lykotrafitis, Topography of native SK channels revealed by force nanoscopy in living neurons, J. Neurosci. 32 (2012) 11435–11440.
[117] P.S. Raman, C.S. Alves, D. Wirtz, K. Konstantopoulos, Single-molecule binding of CD44 to fibrin versus P-selectin predicts their distinct shear-dependent interactions in cancer, J. Cell Sci. 124 (2011) 1903–1910.
[118] S. Sasuga, R. Abe, O. Nikaido, S. Kiyosaki, H. Sekiguchi, A. Ikai, T. Osada, Interaction between pheromone and its receptor of the fission yeast *Schizosaccharomyces pombe* examined by a force spectroscopy study, J. Biomed. Biotechnol. 2012 (2012) 804793.
[119] S. Wielert-Badt, P. Hinterdorfer, H.J. Gruber, J.T. Lin, D. Badt, B. Wimmer, H. Schindler, R.K. Kinne, Single molecule recognition of protein binding epitopes in brush border membranes by force microscopy, Biophys. J. 82 (2002) 2767–2774.
[120] T. Puntheeranurak, L. Wildling, H.J. Gruber, R.K. Kinne, P. Hinterdorfer, Ligands on the string: single-molecule AFM studies on the interaction of antibodies and substrates with the Na^+–glucose co-transporter SGLT1 in living cells, J. Cell Sci. 119 (2006) 2960–2967.
[121] T. Puntheeranurak, B. Wimmer, F. Castaneda, H.J. Gruber, P. Hinterdorfer, R.K. Kinne, Substrate specificity of sugar transport by rabbit SGLT1: single-molecule atomic force microscopy versus transport studies, Biochemistry 46 (2007) 2797–2804.
[122] J. Yu, Q. Wang, X. Shi, X. Ma, H. Yang, Y.G. Chen, X. Fang, Single-molecule force spectroscopy study of interaction between transforming growth factor beta1 and its receptor in living cells, J. Phys. Chem. B 111 (2007) 13619–13625.
[123] A. Kedrov, A.M. Hellawell, A. Klosin, R.B. Broadhurst, E.R.S. Kunji, D.J. Muller, Probing the interactions of carboxy-atractyloside and atractyloside with the yeast mitochondrial ADP/ATP carrier, Structure 18 (2010) 39–46.
[124] L. Ge, C. Perez, I. Waclawska, C. Ziegler, D.J. Muller, Locating an extracellular K^+-dependent interaction site that modulates betaine-binding of the Na^+-coupled betaine symporter BetP, Proc. Natl. Acad. Sci. U. S. A. 108 (2011) E890–E898.
[125] A. Kedrov, S. Wegmann, S.H. Smits, P. Goswami, H. Baumann, D.J. Muller, Detecting molecular interactions that stabilize, activate and guide ligand-binding of the sodium/proton antiporter MjNhaP1 from *Methanococcus jannaschii*, J. Struct. Biol. 159 (2007) 290–301.
[126] A. Kedrov, M. Appel, H. Baumann, C. Ziegler, D.J. Muller, Examining the dynamic energy landscape of an antiporter upon inhibitor binding, J. Mol. Biol. 375 (2008) 1258–1266.
[127] M. Damaghi, C. Bippes, S. Koster, O. Yildiz, S.A. Mari, W. Kuhlbrandt, D.J. Muller, pH-dependent interactions guide the folding and gate the transmembrane pore of the beta-barrel membrane protein OmpG, J. Mol. Biol. 397 (2010) 878–882.
[128] M. Damaghi, K.T. Sapra, S. Koster, O. Yildiz, W. Kuhlbrandt, D.J. Muller, Dual energy landscape: the functional state of the beta-barrel outer membrane protein G molds its unfolding energy landscape, Proteomics 10 (2010) 4151–4162.
[129] C.A. Bippes, A. Zeltina, F. Casagrande, M. Ratera, M. Palacin, D.J. Muller, D. Fotiadis, Substrate binding tunes conformational flexibility and kinetic stability of an amino acid antiporter, J. Biol. Chem. 284 (2009) 18651–18663.